Combustion and Flame 157 (2010) 618–631

Contents lists available at ScienceDirect

Combustion and Flame

journal homepage: www.elsevier.com/locate/combustflame

Feature Article

Negative pressure dependence of mass burning rates of $H_2/CO/O_2$/diluent flames at low flame temperatures

Michael P. Burke *, Marcos Chaos [1], Frederick L. Dryer, Yiguang Ju

Department of Mechanical and Aerospace Engineering, Princeton University, Princeton, NJ 08544, USA

ARTICLE INFO

Article history:
Received 20 June 2009
Received in revised form 25 August 2009
Accepted 25 August 2009
Available online 8 October 2009

Keywords:
Hydrogen
Syngas
Flame speed
Burning velocity
Negative reaction order
High pressure
Low flame temperature
Kinetic mechanism

ABSTRACT

Experimental measurements of burning rates, analysis of the key reactions and kinetic pathways, and modeling studies were performed for $H_2/CO/O_2$/diluent flames spanning a wide range of conditions: equivalence ratios from 0.85 to 2.5, flame temperatures from 1500 to 1800 K, pressures from 1 to 25 atm, CO fuel fractions from 0 to 0.9, and dilution concentrations of He up to 0.8, Ar up to 0.6, and CO_2 up to 0.4. The experimental data show negative pressure dependence of burning rate at high pressure, low flame temperature conditions for all equivalence ratios and CO fractions as high as 0.5. Dilution with CO_2 was observed to strengthen the pressure and temperature dependence compared to Ar-diluted flames of the same flame temperature. Simulations were performed to extend the experimentally studied conditions to conditions typical of gas turbine combustion in Integrated Gasification Combined Cycle processes, including preheated mixtures and other diluents such as N_2 and H_2O.

Substantial differences are observed between literature model predictions and the experimental data as well as among model predictions themselves – up to a factor of three at high pressures. The present findings suggest the need for several rate constant modifications of reactions in the current hydrogen models and raise questions about the sufficiency of the set of hydrogen reactions in most recent hydrogen models to predict high pressure flame conditions relevant to controlling NO_x emissions in gas turbine combustion. For example, the reaction $O + OH + M = HO_2 + M$ is not included in most hydrogen models but is demonstrated here to significantly impact predictions of lean high pressure flames using rates within its uncertainty limits. Further studies are required to reduce uncertainties in third body collision efficiencies for and fall-off behavior of $H + O_2(+M) = HO_2(+M)$ in both pure and mixed bath gases, in rate constants for HO_2 reactions with other radical species at higher temperatures, and in rate constants for reactions such as $O + OH + M$ that become important under the present conditions in order to properly characterize the kinetics and predict global behavior of high-pressure H_2 or H_2/CO flames.

1. Introduction

The H_2/O_2 reaction system is a fundamental topic in combustion science that has historically received significant attention due to both its rich kinetic behavior and its importance to a variety of applications in energy conversion. Since H_2 and its intermediate oxidation species are also intermediate species in the oxidation of all hydrocarbon and oxygenated fuels, the H_2/O_2 mechanism forms an essential subset of any hydrocarbon or oxygenate oxidation mechanism [1]. Recently, there has also been considerable interest in H_2 (either pure or mixed with predominantly CO, CO_2, and H_2O) as a fuel itself as synthetic gas or "syngas" from coal or biomass gasification. Integrated Gasification Combined Cycle (IGCC) processes involve gasifying a solid hydrocarbon feedstock to produce syngas that is typically combusted in gas turbine engines. Such processes offer promise for efficient, low-emission power generation with increased potential for carbon capture and storage (CCS) compared to conventional coal technologies. Lean, premixed combustion of syngas with dilution allows for reduction of the peak flame temperature to lower NO_x emissions. However, fully premixed combustion has not been utilized in commercial syngas applications due to a number of technical challenges associated with the approach, including blowout, flashback, auto-ignition, and combustion dynamics [2]. As a result of interest in and difficulties associated with gas turbine syngas combustion, robust fluid dynamic as well as chemical kinetic modeling tools are sought that are thoroughly validated against experiments spanning a wide range of operating conditions. The

* Corresponding author. Fax: +1 609 258 6109.
E-mail addresses: mpburke@princeton.edu (M.P. Burke), mchaos@princeton.edu, marcos.chaos@fmglobal.com (M. Chaos), fldryer@princeton.edu (F.L. Dryer), yju@princeton.edu (Y. Ju).
[1] Present address: Fire and Explosions Dynamics Group, Fire Hazards and Protection Area, FM Global Engineering and Research, 1151 Boston-Providence Turnpike, P.O. Box 9102, Norwood, MA 02062, USA.

0010-2180/$ - see front matter © 2009 The Combustion Institute. Published by Elsevier Inc. All rights reserved.
doi:10.1016/j.combustflame.2009.08.009

ultimate goal of these modeling efforts is to achieve accurate predictive behavior of dynamic combustor features necessary for reliable operation [3].

There is general confidence in the combustion community in the H_2 mechanism and a perception among some that all H_2 oxidation models are essentially the same in terms of their prediction characteristics. One might conclude that in terms of flame predictions, kinetic uncertainties are sufficiently small as to now be of little importance, though there has been a scarcity of high pressure flame data particularly at low flame temperature conditions. However, it appears that most applications stress a region of parameter space where flame properties are strongly sensitive to a number of reactions that have large uncertainties in their temperature and pressure dependence. Like most applications, syngas combustion in gas turbines employs higher pressures (10 to 30 atm) to improve efficiencies and lower flame temperatures to reduce NO_x emissions (below 1800 K). The higher pressures, lower flame temperatures, and high three-body collision efficiencies of common syngas diluents such as CO_2 and H_2O produce a kinetic regime which is largely controlled by HO_2 and H_2O_2 pathways. Measurements of pure H_2 (e.g. Refs. [4–6]) and H_2/CO (e.g. [7–9]) burning velocities have been mostly studied at atmospheric conditions. A number of recent advancements in flame speed measurement methodologies have resulted in a substantial extension in the range of initial parameters and mixture compositions that can be studied, particularly for high pressure conditions. Each of these recent high pressure studies [10–14] has revealed noteworthy disagreement between experimental data and model predictions.

Several years ago, Tse et al. [10] devised a constant-pressure dual-chambered cylindrical bomb apparatus, extending the pressure range for the stretch-corrected spherical flame method by nearly an order of magnitude. They noted differences between their measured H_2 burning rates at pressures up to 20 atm and those predicted by the model of Mueller et al. [15]. These differences were reconciled in the subsequently presented H_2 models [16–21], many of which involved modification of the $H + OH + M = H_2O + M$ reaction rate constant [16–18]. However, even with these modifications, there still appears to be great difficulty associated with predicting flame behavior at higher pressures. More recently, Sun et al. [12] presented an H_2/CO model validated against their own high-pressure H_2/CO flame speed data up to 40 atm, but predictions with this model do not agree well with the high-pressure H_2 burning rate data of Tse et al. [10] as pointed out by Chaos and Dryer [22]. Bradley et al. [11] conceived a method to extract planar burning velocities from wrinkled outwardly-propagating flames and employed the technique to measure burning velocities of lean H_2–air flames up to 10 atm. They found discrepancies between their derived burning velocities and model predictions. Natarajan et al. [13,14,23] demonstrated that the Bunsen flame approach for flame speed measurement yields values that are consistent with other, more widely accepted methodologies. Flame speeds were determined using conical H_2/CO/CO_2/He flames at pressures to 15 atm and preheat temperatures to 700 K. They identified disagreement between recent kinetic models from Refs. [17,18,24] and their flame speed measurements of preheated, lean H_2/CO flames at pressures up to 15 atm. They cited the temperature dependence of the $H + HO_2 = OH + OH$ reaction as the likely source of disagreement.

In a study of transient effects arising from ignition in a homogeneous mixture, Chen et al. [25] found that unsteady and non-linear effects are substantial for small, spherical flames of non-unity Lewis number. Burke et al. [26] and Chen et al. [27] showed that flame speeds observed close to the wall in cylindrical and spherical chambers are systematically lower due to confinement of the flow field. Correction techniques were developed that extend the flame radius range that can be used for accurate determinations of flame speed allowing for burning velocity measurements of dilute mixtures with prolonged ignition transients. The techniques of Burke et al. [26] and Chen et al. [25] permitted the present experimental study of the burning rates of H_2/CO/O_2/diluent flames up to 25 atm at low flame temperature conditions.

In the present study, we find similar discrepancies between experimental data and model predictions. However, our analyses indicate that the problem could be considerably more involved—complicated by large uncertainties in the temperature and pressure dependences of several key reactions and perhaps even deficiencies in the common H_2/O_2 mechanism reaction set. For example, the reaction $O + OH + M = HO_2 + M$ is not included in nearly all H_2 models but shows strong sensitivity at high pressure, lean conditions (see Fig. 20 below).

The objectives of the present study are threefold. First, we test the performance of recent kinetic models [12,17–21,24] for flame conditions relevant to syngas applications. We present flow-corrected burning rates of H_2/CO/O_2/diluent flames over wide ranges of equivalence ratios, pressures, flame temperatures, and CO and CO_2 concentrations. We focus our study on low flame temperature conditions (below 1800 K) of practical interest to advanced gas turbine applications to achieve low NO_x emissions. While combustion in most applications occurs under lean conditions, we study here both lean and rich mixtures, since reactions important for rich conditions such as those that control the consumption of H atoms are also important for lean conditions, for which reactions that control the consumption of OH radicals are also significant (see Fig. 15 below). Studying a wide range of equivalence ratios aids in de-convolving the sources of disagreement between model and experiment. Second, we explore the changing kinetic pathways in H_2/CO/O_2/diluent flames as pressure is increased to gain a better understanding of the fundamental kinetic phenomena in high pressure flames. Third and finally, we outline possible sources of disagreement between the model predictions and experimental data.

2. Experimental methods

Experiments were conducted in a dual-chambered, pressure-release type high-pressure combustion apparatus (see Fig. 1). The complete details of the experimental apparatus and procedure can be found in Refs. [26,28]. In the present study, the device was operated in the "closed" configuration as discussed in Ref. [26], such that the combustion chamber can be treated as a constant-volume cylindrical bomb.

Mixtures were prepared using the partial pressure method with H_2 (99.99%), CO (99.99%), O_2 (99.5%), He (99.995%), Ar (99.997%), and CO_2 (99.99%). High purity CO stored in an aluminum cylinder was used to ensure no contamination with iron pentacarbonyl, $Fe(CO)_5$, which is readily formed in steel CO cylinders [29] and is a known flame inhibitor [30,31], as discussed in Refs. [3,22,32]. A list of the mixtures studied here is presented in Table 1 for equivalence ratio, φ, pressure, p, nominal flame temperature, $T_{f,\mathrm{nom}}$, and species mole fractions, x. For lean and near stoichiometric cases, He was used as the diluent to increase the Lewis number in order to suppress cellular instability in a similar manner to Tse et al. [10]. For rich cases, Ar or CO_2 was used as the diluent in order to decrease the Lewis number in order to suppress spiraling instability. Diluent concentrations were adjusted to vary adiabatic flame temperatures at fixed equivalence ratio and/or CO fuel fraction. The initial temperature of each experiment was 295 ± 3 K. The mixtures were allowed to homogenize for at least 30 min prior to ignition. The combustible mixture was ignited by a spark discharge across two tungsten electrodes at the center of the chamber.

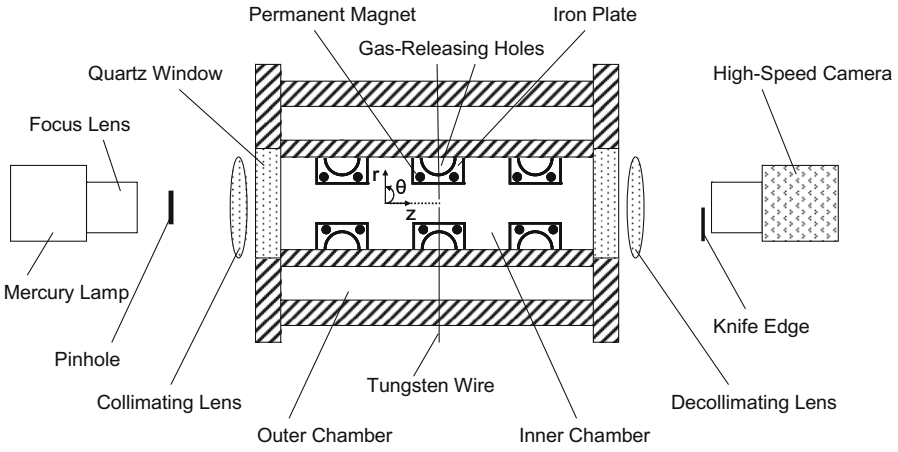

Fig. 1. Diagram of experimental apparatus.

Table 1
Experimental conditions. Initial temperature is 295 K.

φ	$T_{f,\mathrm{nom}}$ (K)	p (atm)	x_{H2}	x_{CO}	x_{O2}	x_{HE}	x_{Ar}	x_{CO2}
0.85	1600	1 to 25	0.1197	0.0000	0.0704	0.8099	0.0000	0.0000
1.0	1500	1 to 10	0.1093	0.0000	0.0546	0.8361	0.0000	0.0000
1.0	1600	1 to 25	0.1183	0.0000	0.0592	0.8225	0.0000	0.0000
1.0	1700	1 to 25	0.1282	0.0000	0.0641	0.8077	0.0000	0.0000
1.0	1800	1 to 20	0.1379	0.0000	0.0690	0.7931	0.0000	0.0000
2.5	1500	1 to 20	0.2941	0.0000	0.0588	0.0000	0.6471	0.0000
2.5	1600	1 to 25	0.3221	0.0000	0.0644	0.0000	0.6134	0.0000
2.5	1700	1 to 25	0.3521	0.0000	0.0704	0.0000	0.5775	0.0000
2.5	1800	1 to 5	0.3846	0.0000	0.0769	0.0000	0.5385	0.0000
2.5	1600	1 to 25	0.1557	0.1557	0.0623	0.0000	0.6264	0.0000
2.5	1600	1 to 20	0.0295	0.2655	0.0590	0.0000	0.6460	0.0000
2.5	1500	1 to 25	0.5182	0.0000	0.1036	0.0000	0.0000	0.3782
2.5	1600	1 to 25	0.5495	0.0000	0.1099	0.0000	0.0000	0.3406
2.5	1700	1 to 25	0.5780	0.0000	0.1156	0.0000	0.0000	0.3064
2.5	1800	1 to 25	0.6061	0.0000	0.1212	0.0000	0.0000	0.2727

High-speed Schlieren photography was utilized for imaging the flame propagation.

From the images, the flame front was located and the flame radius, r_f, was obtained using an automated detection program for ease of processing and reduction of human bias. The raw flame radius data were smoothed and flame front velocity, dr_f/dt, was calculated using local, least-squares 2nd order polynomial fitting methods for data within 3 mm of the radius of interest. The data processed in this manner were consistent with the raw data as well as data processed through a more conventional local-averaging (low-pass) filter.

The instantaneous flame speed, s_u, [26] and stretch rate, κ, [33] were calculated from the flame radius and flame front velocity using

$$s_u = \frac{\frac{1}{\sigma}\frac{dr_f}{dt}}{\left(1+\frac{\sigma-1}{\sigma}\varpi\right)} \tag{1}$$

$$\kappa = \frac{2}{r_f}\frac{dr_f}{dt} \tag{2}$$

where the flow correction term, ϖ, from Ref. [26] was employed in order to account for the actual induced gas motions, instead of using the conventional zero burned gas velocity assumption ($\varpi = 0$). The ratio of unburned to burned gas densities, σ, was calculated using the PREMIX code [34] with the thermochemical parameters of Li et al. [17]. The unstretched flame speed, s_u^o, was obtained through linear extrapolation to zero stretch using the linear stretch relation [35]

$$s_u = s_u^o - L_u \cdot \kappa \tag{3}$$

The data range used for analysis was carefully adjusted for each set of conditions to minimize the effects of confinement and pressure rise [26,27], transient [25] and non-linear behavior [36], cellular instabilities and wrinkling [11,37], spiraling instabilities [38], and buoyancy [39]. Experiments, which were observed to be wrinkled due to cellular or spiraling instabilities, affected by gravity, or influenced by transient or non-linear response of the flame speed to stretch rate, were not considered for further analysis. Only data for which the flame speed–stretch relationship was linear were used for linear extrapolation to zero stretch in order to achieve accurate values for burning velocity. In general, flames always larger than 0.5 cm and always smaller than 2.5 cm in radius were used for analysis; exact ranges used for each measurement and the derived mass burning rate values are reported in Table A1 in the Supplementary material.

The flame images observed and data analysis procedure performed for a $H_2/O_2/Ar$ mixture of equivalence ratio 2.5 and flame temperature near 1600 K at various pressures are shown here as representative cases. Fig. 2 shows the flame surface structure for 1, 15, and 25 atm at a flame radius of 2.5 cm. For 1 atm (a), the flame surface is completely smooth. For 15 atm (b) and 25 atm (c), cracks on the flame surface resulting from the ignition event were retained throughout flame propagation. New cells did not appear for flame radii less than 2.5 cm after an early period influenced by the electrodes, indicating that the linear relationship between stretch rate and flame speed is applicable as concluded by Rozenchan et al. [37]. Our experimental observations (such as those presented in Fig. 3) are consistent with their conclusion.

Fig. 3 shows experimental measurements of instantaneous flame speeds as a function of stretch rate for 0.5 cm < r_f < 2.5 cm and the associated extrapolations for various pressures using the range 1.0 cm < r_f < 2.5 cm. At 1 atm and to a lesser extent at 5 atm, the flame exhibits strong transient and/or non-linear behavior in the flame speed for r_f < 1 cm. Therefore, extrapolation to zero stretch was performed only for r_f > 1 cm. For pressures above 10 atm, the flame speed–stretch relationship remains linear over the entire observed range. For all conditions, the extrapolation lines agree well with the experimental data.

All experimental results presented here for flame speed, s_u^o, or mass burning rate, f^o (defined below), are plotted with error bars calculated from the RMS sum of the uncertainties in s_u^o or f^o corresponding to uncertainties in the measurement of r_f vs. t and calcu-

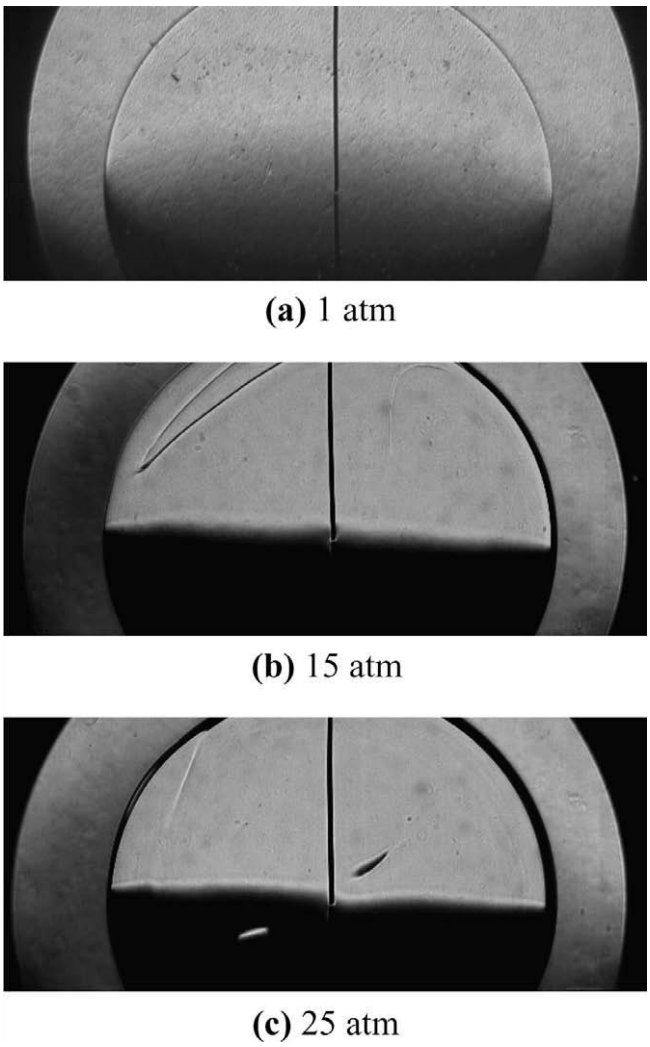

Fig. 2. Schlieren images of propagating flames at r_f = 2.5 cm for an H_2/O_2/Ar mixture of equivalence ratio 2.5 and flame temperature of ~1600 K for various pressures.

lation of s_u^o using a flow correction for a given mixture [26], and uncertainties in the initial conditions reported in Table 1 (i.e. mixture concentrations, temperature and pressure) estimated using the model of Li et al. [17]. Experiments were repeated at least once for nearly all conditions studied here, yielding values well within the reported uncertainty for the measurements.

3. Results

3.1. Pressure dependence of mass burning rates of H_2 flames

Experiments were conducted over a wide range of equivalence ratios, dilution ratios, and pressures. Mass burning rates, defined as

$$f^o = \rho_u s_u^o \tag{4}$$

where ρ_u is the unburned gas density, are presented here since they are typically more illuminating of the global chemistry. As indicated by Egolfopoulos and Law [40], the pressure dependence of the mass burning rate is more directly related to the pressure dependence of the global reaction rate, ω, than the flame speed, which is also dependent on the change of unburned density with pressure. The pressure and temperature dependence of the global reaction rate are represented by an overall reaction order, n, and activation energy, E_a, viz.

$$\omega \sim p^n \exp\left(-E_a/R^o T_f\right) \tag{5}$$

Since the mass burning rate varies with the square root of the reaction rate, the pressure and temperature dependence of the mass burning rate to first order are given by

$$f^o \sim p^{n/2} \exp(-E_a/2R^o T_f) \tag{6}$$

Of particular interest is the dependence of mass burning rate on pressure, which is represented by the overall reaction order, n, defined as [40]

$$n = 2\left\{\frac{\partial \ln(f^o)}{\partial \ln(p)}\right\}_{T_f} \tag{7}$$

for flames with mass burning rate, f^o, pressure, p, and flame temperature, T_f. Mass burning rates measured for H_2/O_2/diluent mixtures at lean and rich conditions of flame temperatures near 1600 K for a variety of pressures are presented in Figs. 4 and 5. At low pres-

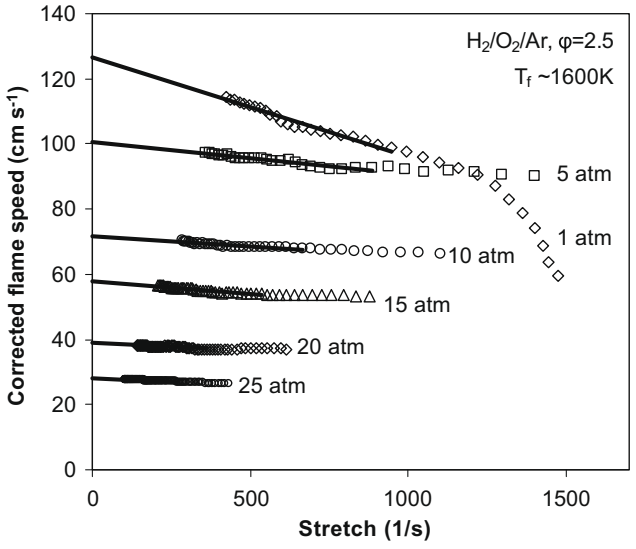

Fig. 3. Experimental flame speed data (symbols) as a function of stretch rate for H_2/O_2/Ar flames of equivalence ratio 2.5 and flame temperature of ~1600 K at various pressures. Lines show linear extrapolations to zero stretch.

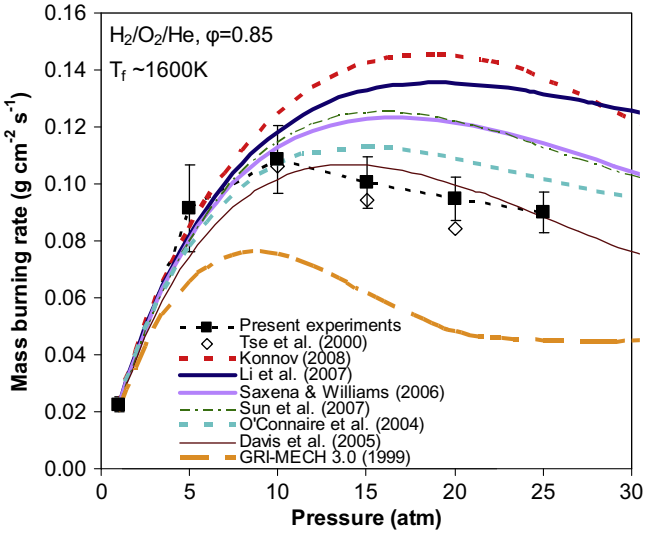

Fig. 4. Mass burning rate measurements from the present study and from Ref. [10] for various pressures for H_2/O_2/He flames of equivalence ratio 0.85 and flame temperature of ~1600 K. Lines show predictions from the different models considered in this study [12,17–21,24].

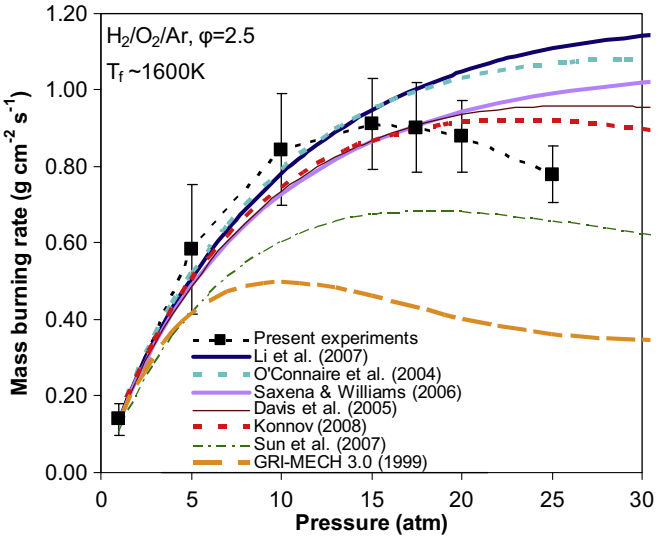

Fig. 5. Mass burning rate measurements for various pressures for $H_2/O_2/Ar$ flames of equivalence ratio 2.5 and flame temperature of ~1600 K. Lines show predictions from the different models considered in this study [12,17–21,24].

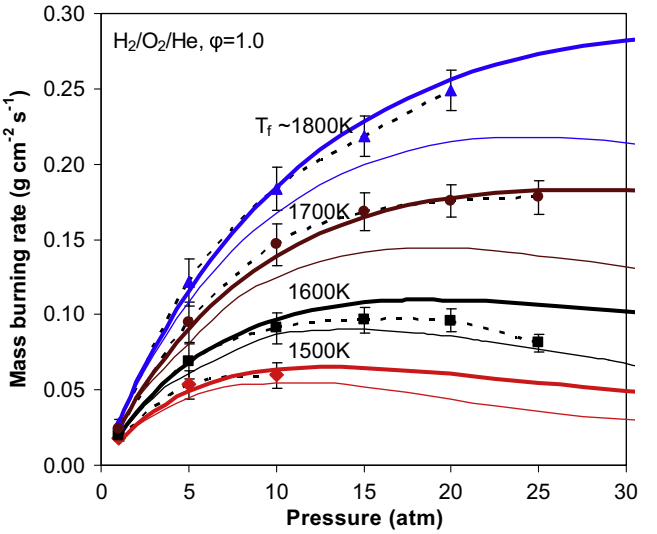

Fig. 6. Pressure dependence of mass burning rates for $H_2/O_2/He$ flames of equivalence ratio 1.0 for various He concentrations. Symbols show experimental data, thick lines show predictions from Li et al. [17], and thin lines show predictions of Davis et al. [18].

sures up to ~10 atm, the reaction order is experimentally observed to be positive, while at pressures above 10 to 15 atm, the reaction order is found to be negative. The variations of overall reaction order with pressure are qualitatively similar, but differ quantitatively for lean and rich conditions. Negative reaction orders in flames are not common but have been experimentally observed previously in N_2-diluted CH_4–air flames [40,41].

At lower pressures, predictions using recently published chemical kinetic models agree reasonably well with one another and the experimental data. However, at higher pressures, the predicted mass burning rates differ substantially from model to model and with experimental data. Much larger disparities are apparent among model predictions themselves at fuel-rich conditions, with variations of nearly a factor of three in predicted burning rates. Given that the H_2 kinetic models investigated here were all validated against a wide range of (and frequently the same) data from numerous experimental apparatuses including the high pressure flame speeds of Tse et al. [10], the disparities noted amongst the predictions and with the present experimental results are noteworthy.

3.2. Flame temperature dependence of mass burning rates of H_2 flames

Mass burning rates for H_2/O_2/diluent mixtures of different flame temperatures were measured for pressures from 1 to 25 atm for equivalence ratios of 1.0 and 2.5. The mass burning rate of H_2/O_2/He mixtures of equivalence ratio 1.0 and flame temperatures of 1500, 1600, 1700, and 1800 K are plotted in Fig. 6. The mass burning rate is higher for higher temperatures. Negative pressure dependences were observed for the 1600 K case but not for higher temperatures over the pressure range studied. The mass burning rate of $H_2/O_2/Ar$ mixtures of equivalence ratio 2.5 and flame temperatures of 1500, 1600, 1700, and 1800 K are plotted in Fig. 7. Similar to the stoichiometric case, the mass burning rate is higher for higher temperatures. Negative reaction orders were observed for the 1500 and 1600 K cases but not for higher temperatures over the pressure range studied. The pressure of the maximum burning rate decreases with decreasing flame temperature. Disagreement between the experimental data and model predictions is largest at higher pressures and lower flame temperatures.

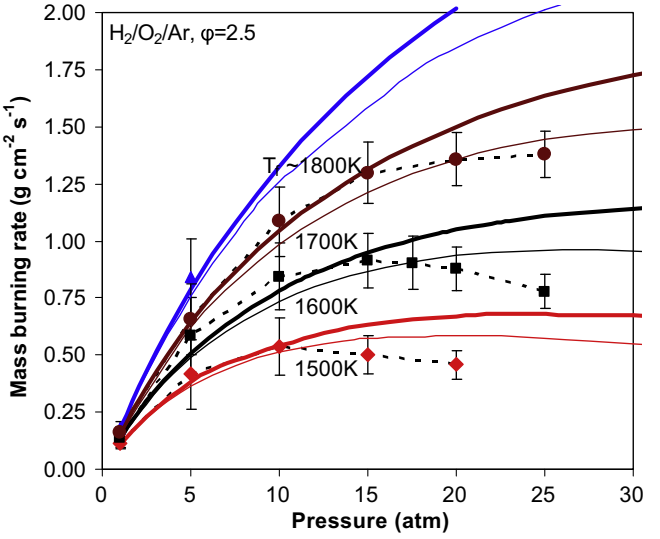

Fig. 7. Pressure dependence of mass burning rates for $H_2/O_2/Ar$ flames of equivalence ratio 2.5 for various Ar concentrations. Symbols show experimental data, thick lines show predictions from Li et al. [17], and thin lines show predictions of Davis et al. [18].

The temperature dependences of the mass burning rates of H_2/O_2/diluent mixtures at various pressures of equivalence ratios 1.0 and 2.5 are plotted in Figs. 8 and 9. The trends observed for both equivalence ratios are similar. The mass burning rate increases with flame temperature. The temperature dependence becomes stronger with increasing pressures—indicative of a higher global activation energy, E_a, defined as [40]

$$E_a = -2R^o \left\{ \frac{\partial \ln(f^o)}{\partial (1/T_f)} \right\}_p \tag{8}$$

as pressure is increased.

The Zeldovich number, defined as [42]

$$Ze = \frac{(T_f - T_u)E_a/R^o}{T_f^2} \tag{9}$$

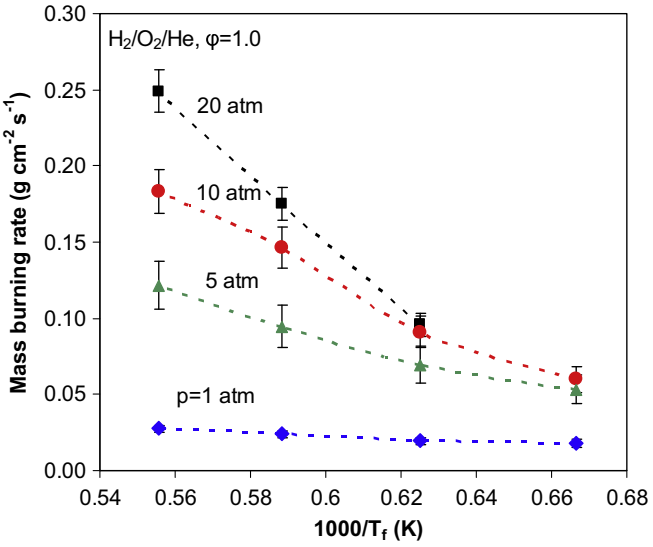

Fig. 8. Flame temperature dependence of mass burning rates for H_2/O_2/He flames of equivalence ratio 1.0 at different pressures.

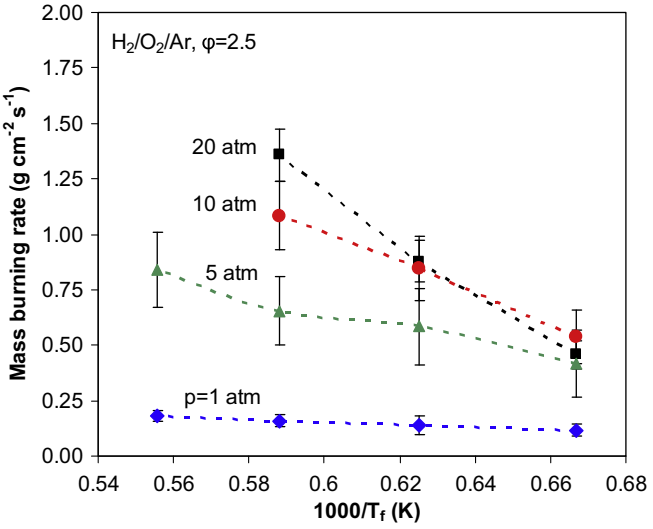

Fig. 9. Flame temperature dependence of mass burning rates for H_2/O_2/Ar flames of equivalence ratio 2.5 at different pressures.

represents a non-dimensional activation energy corresponding in asymptotic theory to the ratio of the overall flame thickness to the reaction zone thickness. (Here, T_u is the unburned gas temperature.) Thus, an increasing Zeldovich number with increasing pressure implies a higher activation energy and smaller reactive portion of the flame. This observation of a stronger temperature dependence, and hence higher activation energy and Zeldovich number, at higher pressures is consistent with the numerical studies described below.

3.3. Effect of CO addition on the pressure dependence of mass burning rates

The pressure dependences of $H_2/CO/O_2$/Ar mixtures of equivalence ratio 2.5 for H_2/CO ratios of 100/0, 50/50 and 10/90 are plotted in Fig. 10. The level of Ar dilution was varied for the mixtures to maintain a flame temperature of approximately 1600 K. Negative pressure dependence is observed for the H_2/CO = 50/50 mixture

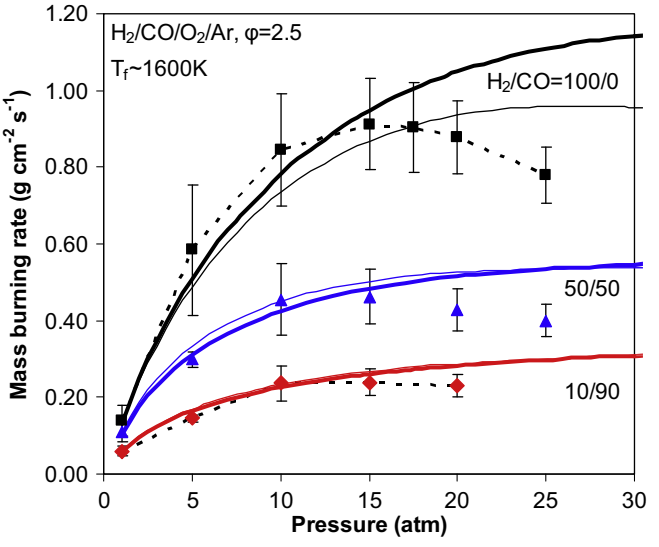

Fig. 10. Pressure dependence of mass burning rates for $H_2/CO/O_2$/Ar flames of equivalence ratio 2.5 for various CO fuel fractions. Symbols show experimental data, thick lines show predictions from Li et al. [17], and thin lines show predictions of Davis et al. [18].

for pressures above 10 to 15 atm – slightly lower than for the pure H_2 mixture. The overall pressure dependence is quite similar for pure H_2 and H_2/CO = 50/50. For H_2/CO = 10/90, the data show that the mass burning rate becomes nearly independent of pressure at pressures above 10 atm. Disagreement between the experimental data and model predictions is strongest at higher pressures for all CO fuel fractions.

The mass burning rate as a function of CO fuel fraction for various pressures is shown in Fig. 11. Higher CO fractions have lower burning rates for all pressures. Additionally, the dependence of CO fuel fraction on the mass burning rate of H_2/CO mixtures is nearly the same for all pressures. For example, the ratio of the mass burning rate of pure H_2 to that of H_2/CO = 10/90 is 2.3 for 1 atm and 3.7 ± 0.5 above 5 atm.

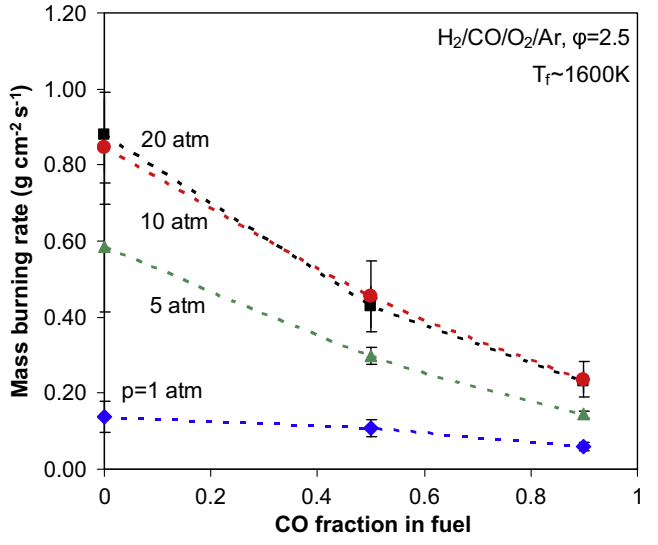

Fig. 11. The CO fuel fraction dependence of mass burning rates for $H_2/CO/O_2$/Ar flames of equivalence ratio 2.5 for different pressures.

3.4. Effect of CO_2 dilution on the pressure and flame temperature dependences of mass burning rates

Mass burning rates for H_2/O_2 mixtures with CO_2 dilution were measured for different flame temperatures and pressures. Dilution with CO_2 is of interest due its high concentrations in synthetic gas mixtures and the expectation that CO_2 amplifies the pressure dependence of the mass burning rate due to its high third body efficiency relative to Ar (~5 to 1 for $H + O_2(+M) = HO_2(+M)$ (R1)).

The pressure dependences of $H_2/O_2/CO_2$ mixtures of equivalence ratio 2.5 for flame temperatures of 1500, 1600, 1700, and 1800 K are plotted in Fig. 12. Negative pressure dependence is observed below 25 atm for all flame temperatures studied. Similar to Ar-diluted mixtures, as the flame temperature is increased the pressure of maximum burning rate is raised. Compared to Ar-diluted mixtures of the same flame temperature, the CO_2-diluted flames exhibit negative pressure dependence at lower pressures and even at higher temperature conditions. Strong disagreement between the model predictions and experimental measurements for mass burning rate is observed above 5 atm. Fig. 13 shows the temperature dependence of CO_2-diluted flames at various pressures. Similar to Ar-diluted flames, the flame temperature dependence of the mass burning rate is stronger at higher pressures. Compared to Ar-diluted flames, however, the temperature dependence is considerably stronger – for example, $E_a = 80$ kcal/mol for CO_2-diluted flames at 20 atm compared to $E_a = 53$ kcal/mol for Ar-diluted flames at 20 atm over the temperature range from 1500 to 1700 K using Eq. (8). Reasons for the stronger temperature and pressure dependence for CO_2-diluted flames compared to Ar-diluted flames are discussed in the next section.

Even though large concentrations of CO_2 were present in the unburned and burned gases, the measured flame speed still demonstrated a linear relationship with stretch rate, i.e. there were no anomalous trends that would suggest significant radiation-induced burned gas motions that affect the determination of the measured flame speed as explored in our previous work [43]. Ju and co-workers showed that radiation absorption and emission are important in flames with high CO_2 dilution, since CO_2 is a strong absorber [44,45]. Chen et al. [44] indicated that spectral-dependent radiation absorption must be included for any quantitative predictions of flame speed with CO_2 dilution. The effect of radiation is not considered in detail here, and we refer the reader to Refs. [44,45] for more information. The flames are approximated as adiabatic in the simulations shown in Fig. 12. Given that disagreement is observed between model predictions and experimental data for $H_2/O_2/Ar$ mixtures as well as between adiabatic predictions using two different kinetic models [17,18] for $H_2/O_2/CO_2$ mixtures, the treatment of radiation in the simulations does not appear to be the sole source of disagreement between model predictions and experimental data.

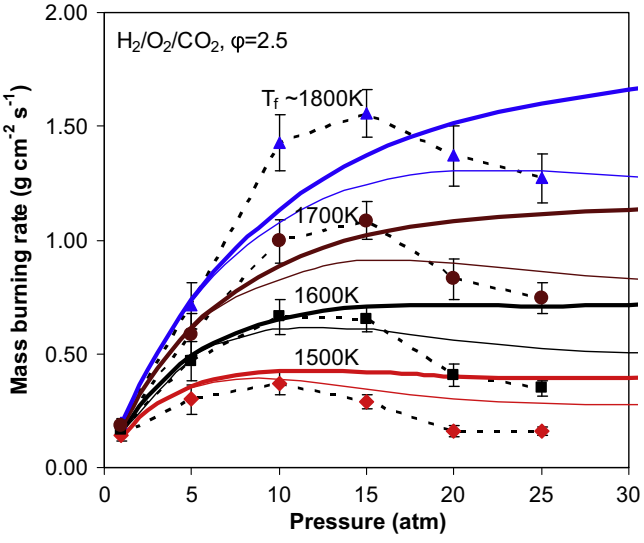

Fig. 12. Pressure dependence of mass burning rates for $H_2/O_2/CO_2$ flames of equivalence ratio 2.5 for various CO_2 concentrations. Symbols show experimental data, thick lines show predictions from Li et al. [17], and thin lines show predictions of Davis et al. [18].

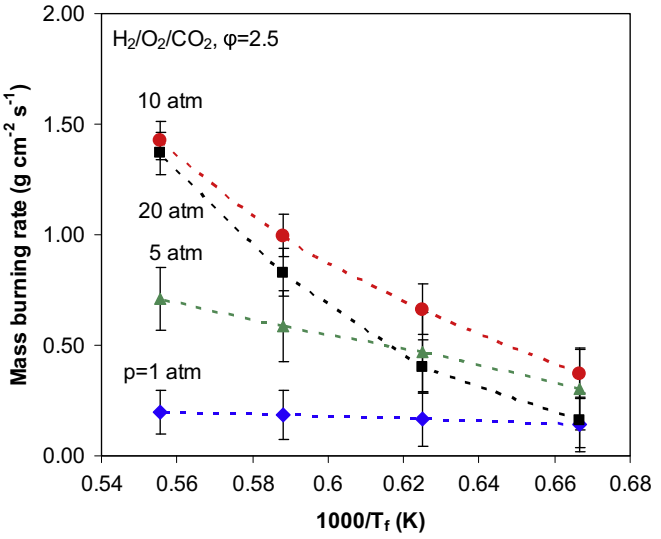

Fig. 13. Flame temperature dependence of mass burning rates for $H_2/O_2/CO_2$ flames of equivalence ratio 2.5 at different pressures.

4. Analysis and discussion

4.1. Analysis of controlling reactions and kinetic pathways

Species profiles and reaction fluxes from predictions using the mechanism of Li et al. [17] were analyzed for the lean and rich conditions of Figs. 4 and 5 at 1, 10, and 20 atm to ascertain the effect of pressure on the flame structure and kinetic pathways. (While comparisons between experimental data and kinetic model predictions indicate significant shortcomings in the kinetic models, we expect model predictions of flame structure and kinetic pathways will be illuminating nonetheless). Flux analyses of the intermediate species in the H_2/O_2 system (H, OH, O, HO_2, and H_2O_2) were conducted. The results indicate that the pressure-dependent reactions that

Table 2
List of reactions discussed in the text.

(R1)	$H + O_2(+M) = HO_2(+M)$
(R2)	$H + OH + M = H_2O + M$
(R3)	$O + H + M = OH + M$
(R4)	$H + H + M = H_2 + M$
(R5)	$H + O_2 = OH + O$
(R6)	$O + H_2 = OH + H$
(R7)	$OH + H_2 = H_2O + H$
(R8)	$HO_2 + H = H_2 + O_2$
(R9)	$HO_2 + H = OH + OH$
(R10)	$HO_2 + OH = H_2O + O_2$
(R11)	$CO + OH = CO_2 + H$
(R12)	$HCO + H = CO + H_2$
(R13)	$H + CO + M = HCO + M$
(R14)	$HCO + O_2 = CO + HO_2$
(R15)	$O + OH + M = HO_2 + M$
(R16)	$H + HO_2 + M = H_2O_2 + M$
(R17)	$HO_2 + HO_2 = H_2O_2 + O_2$

contribute substantially to the flux of H, OH, O, and HO_2 are $H + O_2(+M) = HO_2(+M)$ (R1), $H + OH + M = H_2O + M$ (R2), $O + H + M = OH + M$ (R3) for lean conditions, and $H + H + M = H_2 + M$ (R4) for rich conditions (Table 2 provides a list of the reactions discussed herein). Mole fractions of H, OH, and O are lower at high pressure to such an extent for these low flame temperature conditions that the percent flux of H, OH, and O through the radical–radical recombination reactions (R2)–(R4) is actually less at higher pressures than at lower pressures. While H_2O_2 is formed in appreciable concentrations at 20 atm, reactions that involve H_2O_2 are not responsible for significant production or consumption of any other species in the H_2/O_2 system. Consequently, H_2O_2 pathways do not appear to be important in the flames studied here (though they become important at higher pressures).

The primary cause for the pressure and temperature dependence appears to be the consumption paths of the H atom, as supported below. The main pressure-dependent recombination reaction (R1) competes directly with the main chain branching reaction, $H + O_2 = OH + O$ (R5) for H atoms. At low pressures and temperatures, (R1) is effectively radical chain terminating while (R5) participates in a chain branching loop with $O + H_2 = OH + H$ (R6) and $OH + H_2 = H_2O + H$ (R7), which essentially produces three H atoms for every H atom entered. If (R1) and (R5)–(R7) are considered and (R1) is assumed to be terminating, the overall branching ratio is responsible for the well-known second limit in homogeneous kinetics [46]

$$\frac{2k_5}{k_1[M]} = 1 \tag{10}$$

At pressures above the third explosion limit and lower temperatures such that $2k_5/k_1[M] < 1$, H_2O_2 formation from HO_2 and its subsequent decomposition and/or reaction allows for a reaction sequence that is explosive, but the sequence is chain-carrying and thermally driven in contrast to the faster chain-branching kinetics for $2k_5/k_1[M] > 1$ [15]. Consequently, the second limit plays an important role even for pressures above the third limit in terms of characteristic reaction times. For these temperatures and pressures, HO_2 and H are present in high enough concentrations that HO_2 reacts with H through two competing channels: $H + HO_2 = H_2 + O_2$ (R8) and $H + HO_2 = OH + OH$ (R9). Steady-state analysis of the radical pool considering (R1) and (R5)–(R9) yields a critical branching ratio

$$\frac{k_8 + k_9}{2k_8}\frac{2k_5}{k_1[M]} = 1, \tag{11}$$

that demarcates straight-chain from chain-branching kinetics, typically called the "extended" second limit [15,47,48]. The demarcation has been observed in flow reactor species profiles [15,47] and counterflow ignition studies [48]. The four reactions involved in the extended second limit, (R1), (R5), (R8), and (R9), also play an important role in the pressure dependence of high pressure flame kinetics, as demonstrated below.

The effect of pressure on the flame structure based on the flux of H atoms through the two pairs of competing pathways, (R1) & (R5) and (R8) & (R9), as well as H atom mole fraction is illustrated in Fig. 14. This figure also shows the temperature of the extended second limit for the given pressures. The results indicate that with increasing pressure, the temperature of extended second limit increases accordingly, moving significantly toward the post-flame region for lean and rich mixtures. Therefore, the portion of the flame that undergoes strong branching kinetics (i.e. at temperatures above the extended second limit) is reduced to a smaller temperature window at higher pressures. As pressure is increased, the flux through (R1) relative to (R5) is increased, producing more HO_2 radical instead of O atom and OH radical. The higher HO_2 concentrations lead to increased flux through (R8) and (R9) compared to (R5) as well. Overall,

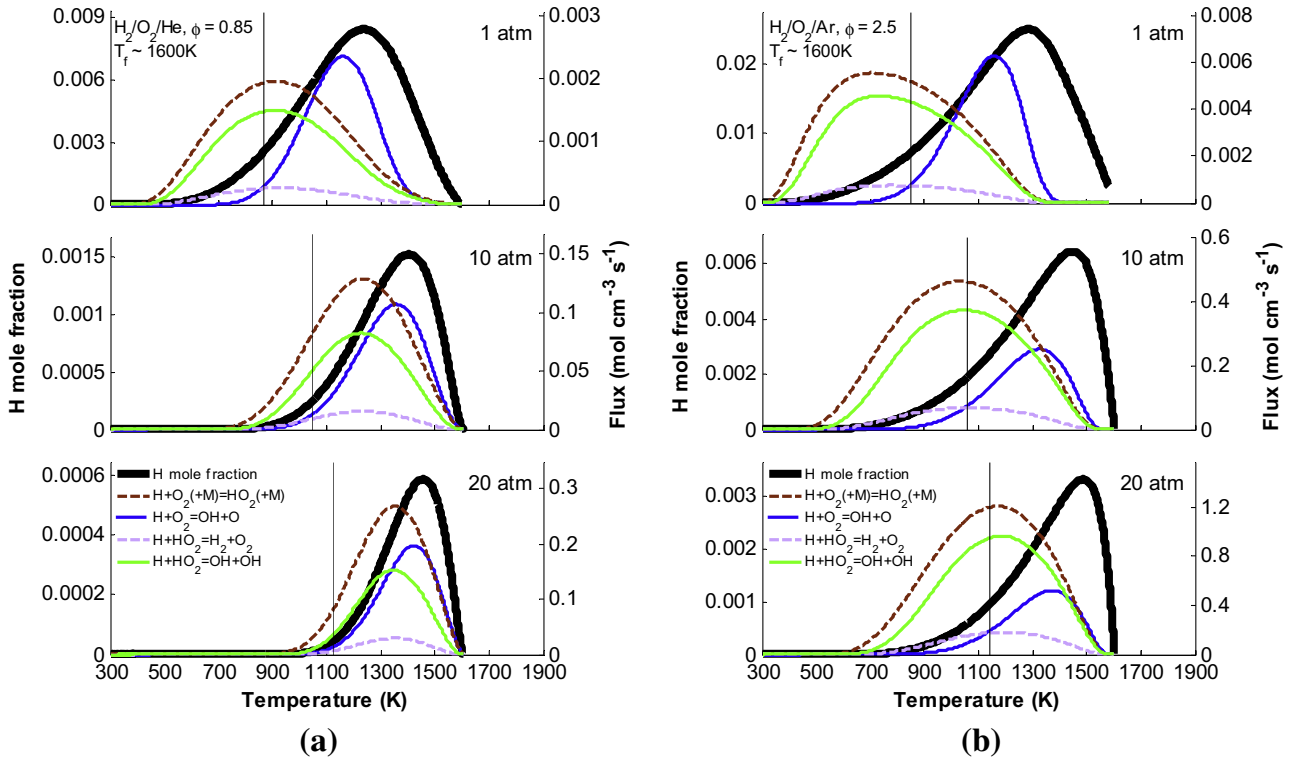

Fig. 14. H radical mole fraction and H consumption by $H + O_2(+M) = HO_2(+M)$ (R1), $H + O_2 = OH + O$ (R5), $HO_2 + H = H_2 + O_2$ (R8), and $HO_2 + H = OH + OH$ (R9): (a) H_2/O_2/He flames of equivalence ratio 0.85 with flame temperature of ~1600 K (same conditions as Fig. 4); (b) H_2/O_2/Ar flames of equivalence ratio 2.5 with flame temperature of ~1600 K (same conditions as Fig. 5). Vertical lines mark the temperature of the extended second limit for the given pressures.

there is more flux through the HO_2 channels instead of strong branching channels at higher pressures. The peak H atom mole fraction is decreased substantially and also moves toward the post-flame region with increasing pressure. Furthermore, the reaction zone region in which (R1) and (R5) compete is restricted to higher temperatures and a smaller overall temperature range as pressure is increased. Similar shifts toward smaller, higher temperature windows occur in the flux profiles of other controlling reactions, including (R8) and (R9), as well as other radical and reaction flux profiles. Such a restriction of the strongly reactive portion of the flame to higher temperatures can be expressed as an increase in the overall activation energy or Zeldovich number of the mixture with pressure. The narrower, higher temperature window at higher pressures of the bulk reactivity predicted by the simulations serves to explain the stronger temperature dependence of the mass burning rate at higher pressures observed in the experiment.

Comparing Fig. 14a and b, the responses of the flame structure to pressure are different for different equivalence ratios. The peak fluxes of the H atom through (R1) and (R5) occur closer to the unburned region in rich flames, where the concentration of oxygen is higher. Since the peak flux of the H atom occurs at lower temperatures, where (R5) is favored relative to (R1), the peak flux through (R5) relative to (R1) is higher compared to lean conditions. At both lean and rich conditions, the mole fraction of HO_2 compared to H is substantially higher at higher pressures as a much larger portion of the temperature profile is below the extended second limit temperature where (R1) is favored. Consequently, pathways involving HO_2 play a much larger role in the overall kinetics, as illustrated for rich conditions by the increased percentage of the flux through (R8) and (R9) at higher pressures in Fig. 14b.

Analyses conducted using the mechanism of Li et al. [17] indicate that sensitivity of mass burning rate predictions, for the conditions shown in Figs. 4 and 5, to elementary rates increases considerably with pressure, as demonstrated in Fig. 15. The reactions, to which the pressure dependence for rich conditions is most sensitive, are primarily reactions that involve H atoms, namely (R1), (R5), (R8), and (R9) (Fig. 15b). Rates of these four reactions define the extended second explosion limit, as discussed above. The reactions that appear to govern the pressure dependence for lean conditions are the reactions discussed above in addition to reactions involving OH radicals, namely $HO_2 + OH = H_2O + O_2$ (R10) and $H_2 + OH = H_2O + H$ (R7), as well as $O + H_2 = H + OH$ (R6) and $H + OH + M = H_2O + M$ (R2) (Fig. 15a). Even at lean conditions, however, the rate of the branching reaction (R5) exhibits the strongest sensitivity. Reaction (R10) competes with (R8) and (R9) for HO_2 radicals and (R7) for OH radicals and inhibits the overall kinetics by converting two radicals to stable species.

In a similar manner to increasing pressure, decreasing the flame temperature through dilution restricts the reactive portion of the flame to a narrower temperature window, where branching and recombination channels are more competitive. Since recombination reactions are favored with increasing pressure and decreasing flame temperature, flux through recombination and branching channels can become roughly equal through the most reactive portion of the flame at high pressures and low flame temperatures. As a result, the sensitivity of the predictions to the rate parameters for those reactions increases dramatically. Indeed, *A*-factor sensitivity analyses (not shown here) of different flame temperature conditions indicate similar reaction sensitivity rankings but different magnitudes for sensitivity indices. As flame temperature is decreased, the sensitivity indices increase significantly.

Since preheated mixtures are of interest to practical IGCC systems, flame simulations were performed to discern the effect of preheat on the mass burning rate pressure dependence and prediction sensitivities to rate parameters. Two H_2/O_2/He mixtures of equivalence ratio 0.85 were studied with a preheat temperature of 700 K, characteristic of isentropic compression of air from 1 to 20 atm. For one mixture, the He dilution was varied to maintain the same flame temperature of 1600 K as the case in Fig. 4. For the other mixture, the He dilution was the same as the case in Fig. 4. For the case of increased dilution to maintain the same flame temperature, the pressure dependence and sensitivity results are nearly identical to the non-preheated case. For the case of fixed dilution, which results in a flame temperature of 2000 K, the burning rate monotonically increases from 1 to 30 atm, and sensitivity analysis reveals the same important reactions but lower sensitivity indices. Therefore, it appears that increasing the flame temperature by increasing the preheat temperature and increasing the flame temperature by decreasing dilution have the same effect on the pressure dependence.

A-factor sensitivity analysis for the burning rate of the rich H_2/CO = 50/50 mixture of Fig. 10 at different pressures, shown in

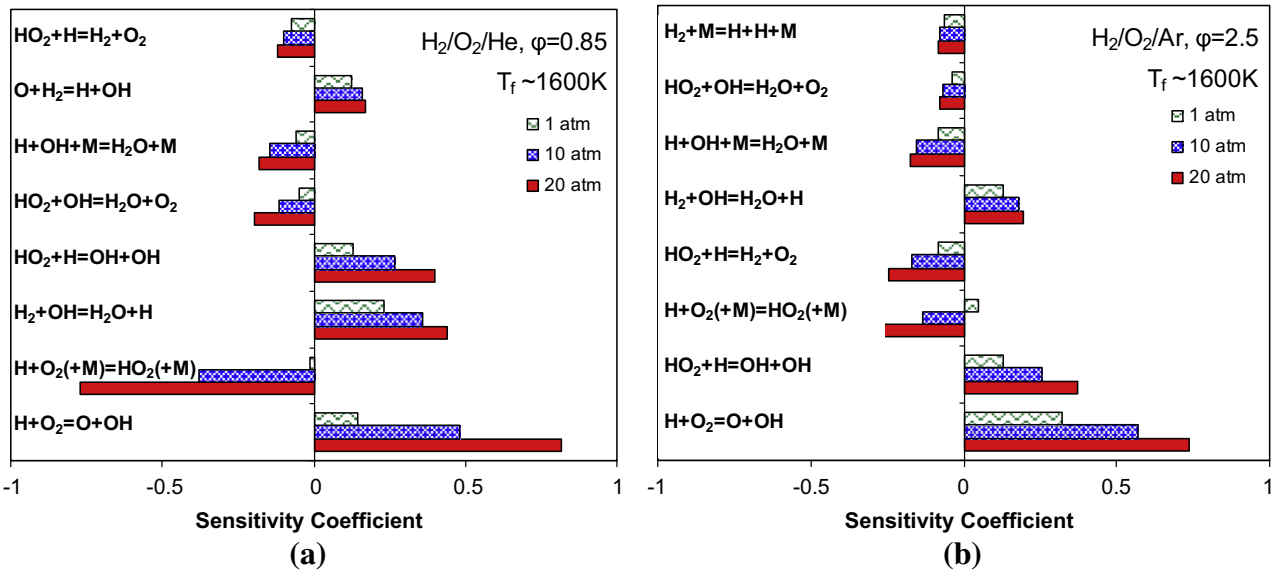

Fig. 15. Sensitivity of mass burning rate to *A*-factors of elementary rates: (a) H_2/O_2/He flames of equivalence ratio 0.85 with flame temperature of ~1600 K (same conditions as Fig. 4); (b) H_2/O_2/Ar flames of equivalence ratio 2.5 with flame temperature of ~1600 K (same conditions as Fig. 5).

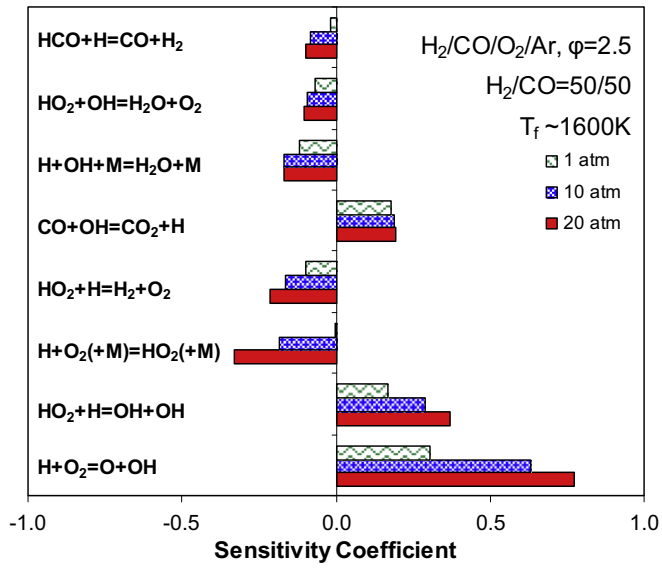

Fig. 16. Sensitivity of mass burning rate to *A*-factors of elementary rates for H_2/CO/O_2/Ar flames (H_2/CO = 50/50) of equivalence ratio 2.5 and flame temperature of ~1600 K (same conditions as Fig. 10).

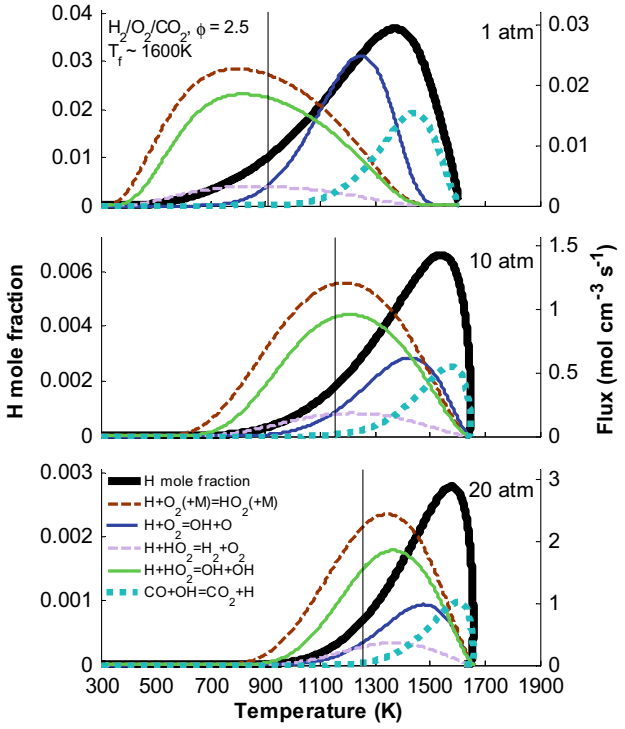

Fig. 17. H radical mole fraction and H consumption by H + O_2(+M) = HO_2(+M) (R1), H + O_2 = OH + O (R5), HO_2 + H = H_2 + O_2 (R8), HO_2 + H = OH + OH (R9), and CO + OH = CO_2 + H (R11) for H_2/O_2/CO_2 flames of equivalence ratio 2.5 with flame temperature of ~1600 K (same conditions as Fig. 12). Vertical lines mark the temperature of the extended second limit.

Fig. 16, reveals a nearly identical reaction sensitivity ranking, pressure dependences, and magnitudes as for the pure H_2 mixture, shown in Fig. 15. The two most notable exceptions are that CO + OH = CO_2 + H (R11) replaces H_2 + OH = H_2O + H (R7) and HCO + H = CO + H_2 (R12) replaces H + H + M = H_2 + M (R4) in the ranking. Additionally the sensitivities of those two reactions, (R11) and (R12), exhibit the same pressure dependence and approximate magnitudes as (R7) and (R4), respectively.

In terms of the effect on the radical pool, (R11) and (R7) are equivalent paths – each consume a parent fuel molecule and an OH radical and produce a stable product and an H atom. At the higher temperatures where peak reaction sensitivities and radical fluxes occur for high pressure flames, (R11) is an order of magnitude slower than (R7). Consequently, it is reasonable to expect that the burning rate will be more sensitive to (R11). Similarly, a combination of H + CO + M = HCO + M (R13) and HCO + H = CO + H_2 (R12) produces a net path for H atom destruction that is essentially equivalent to (R4). For the pure H_2 case, (R4) consumes 7.5% of the H atoms across the entire flame. Whereas for the H_2/CO = 50/50 mixture, (R4) consumes 3.5%, (R13) 5.5%, and (R12) 3%; for the H_2/CO = 10/90 mixture, (R4) consumes 2.5%, (R13) 8.4%, and (R12) 4%. For both H_2/CO mixtures, approximately half of the HCO radicals proceed through (R12) and half through HCO + O_2 = CO + HO_2 (R14).

If the steady-state analysis for the radical pool is extended to include (R11) in addition, the equation for the extended second limit, Eq. (11), is unchanged since (R11) and (R7) both convert OH radicals to H atoms. Since the third body efficiencies of CO and H_2 are quite similar in the expressions of Li et al. for (R1), the extended second limit temperature is not predicted to change substantially. Comparison of H atom concentrations as functions of temperature for H_2/CO = 100/0, 50/50, and 10/90 reveals lower magnitudes for higher CO fuel fractions but similar profiles.

Carbon dioxide is expected to modify the flame kinetics in two main ways. First, the reverse of the reaction CO + OH = CO_2 + H (R11) decreases the H atom concentration and therefore serves to weaken the flame. Second, dilution with CO_2 results in an overall stronger third body efficiency of the mixture than dilution with Ar for the same flame temperature. The stronger third body efficiency of CO_2 relative to He or Ar (~5 to 1 for (R1)) substantially increases the rate of the recombination reaction (R1), which was identified as the pressure-dependent reaction responsible for the most flux of radical species. Additionally, due to the high specific heat of CO_2, lower concentrations of diluent are required to achieve the same flame temperature. Therefore, there are higher reactant concentrations of H_2 and O_2 and consequently higher product concentrations of H_2O. Higher concentrations of H_2O, which has an even stronger third body efficiency of relative to He or Ar (~16 to 1 for (R1) as used in Li et al. [17], ~23 to 1 as recently measured by Michael et al. [49]), further increases the rate of the recombination reaction (R1) near the post-flame region. Flux analysis reveals an increased extended second limit crossover temperature with CO_2 dilution (see Fig. 17) compared to Ar dilution (see Fig. 14b) for the same pressure, flame temperature, and equivalence ratio conditions. Compared to Ar-diluted flames of the same pressure and flame temperature, H atom concentrations and fluxes are shifted to a higher, narrower temperature region for the CO_2-diluted flames – indicative of a higher global activation energy. Additionally, there is increased flux through the recombination reaction (R1) relative to the branching reaction (R5). Since the mixture is fuel-rich, the reverse reaction of (R11) converts CO_2 to CO near the post-flame region to achieve final equilibrium concentrations. During this process, H atoms are converted to OH radicals, thus reducing the available H atom pool further. The above discussion is consistent with the trends observed in experimental data for CO_2 dilution (see Figs. 12 and 13) – a stronger pressure and temperature dependence of the mass burning rate as well as lower pressures of maximum burning rate compared to those of Ar-diluted flames.

Other diluents of interest to IGCC applications, N_2 and H_2O, similarly have high specific heats and high third body efficiencies relative to Ar or He. Consequently, both of these diluents are expected to strengthen the pressure dependence for a certain flame temperature – H_2O, with a third body efficiency relative to He or Ar of ~16

to 1 for (R1) as used in Li et al. [17] or ~23 to 1 as recently measured [49], to a much larger extent than N_2, with a third body efficiency relative to He or Ar of ~2 to 1 for (R1) as used in Li et al. [17] and recently measured [49]. Simulations of H_2/O_2/diluent flames of equivalence ratio 0.85 and dilution levels chosen to yield flame temperatures near 1600 K reveal pressures of maximum burning rate of 20, 10, 5, and 2 atm for He, N_2, CO_2, and H_2O, respectively. Accordingly, the strength of the burning rate pressure dependence of H_2/O_2/diluent flames can be ranked by diluent as He < N_2 < CO_2 < H_2O.

Temperature window sensitivity analyses [50] of burning rate to reaction rate constants as a function of temperature for the lean H_2/O_2/He mixture of Fig. 4 were conducted. In contrast to conventional (*A*-factor) sensitivity analysis where the rate constant is perturbed uniformly across all temperatures, temperature window sensitivity analysis perturbs the rate constant with a narrow Gaussian function centered at a particular temperature. In such a way, a sensitivity index that is a function of temperature is obtained to aid in identifying the temperature range over which a rate constant is most sensitive. The results for HO_2 reactions with H and OH, (R8), (R9), and (R10), are presented in Fig. 18. The temperature window of peak sensitivity to the HO_2 reactions becomes narrower, and moves to higher temperatures as pressure increases. In contrast to a temperature of peak sensitivity around 700 K at 1 atm, at 20 atm the peak sensitivity occurs at a temperature around 1350 K. The same shift in temperature sensitivity with pressure is also observed for all other reactions, with the largest shift occurring for reactions (R8)–(R10) shown in Fig. 18.

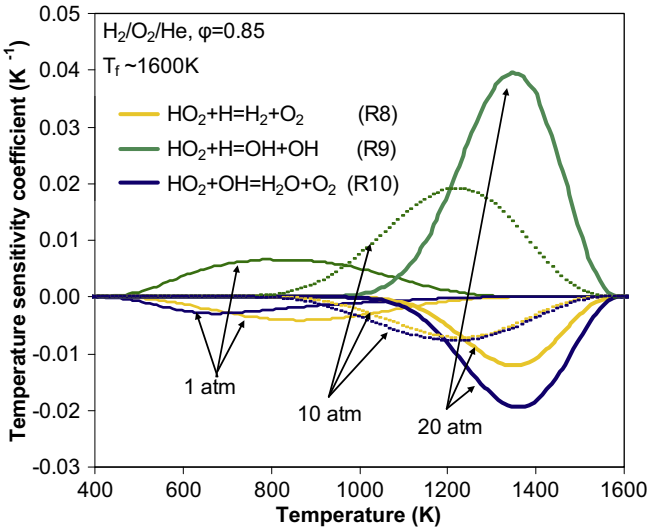

Fig. 18. Temperature window sensitivity of mass burning rate to elementary rates for H_2/O_2/He flames of equivalence ratio 0.85 with flame temperature of ~1600 K at various pressures (same conditions as Fig. 4).

4.2. Implications for kinetic modeling

The observed discrepancies between model predictions [12,17–21,24] and experiments, and among model predictions themselves, are noteworthy. All of the models tested here have been validated against extensive (and frequently the same) sets of data. All of these H_2 models [17–21] have been validated against high pressure burning rate data [10]. Furthermore, many of the most sensitive reactions for the present conditions are highly sensitive reactions in a wide variety of combustion systems, both for H_2 and other hydrocarbons. However, it appears that almost all of the reactions listed in Fig. 15 could potentially contribute to the disagreement in burning rate between experiments and models or among models, as supported below. Here we focus solely on reactions of the H_2/O_2 subset since the problems in predicting H_2/O_2 flame behavior will also be present in $H_2/CO/O_2/CO_2$ flames.

We categorize the most sensitive reactions from Fig. 15 as: (R5)–(R7) and (R1), which are important in nearly all combustion processes and exhibit high sensitivities at the present conditions; HO_2 + radical reactions like (R8)–(R10), which are major pathways at high pressures where HO_2 is present in higher concentrations; and radical–radical recombination reactions like (R2) and potentially $O + OH + M = HO_2 + M$ (R15) and $H + HO_2 + M = H_2O_2 + M$ (R16), which are important in high pressure flames where concentrations of both radicals and collision partners is higher. The effect of these reactions on predicting mass burning rates for flames studied here is discussed below.

The reactions (R1) and (R5)–(R7) are among the most important and well-characterized reactions in combustion kinetics. While the uncertainties in their associated rate constants are quite low [51], the high burning rate sensitivities for the present conditions amplify the effects of these uncertainties substantially in the mass burning rate predictions. As a demonstration, Fig. 19 shows mass burning rate predictions using the model of Li et al. with (R5) at its upper and lower uncertainty limits provided by Baulch et al. [51], ln (*A*) = 0.2 at 3500 K. Predictions using the upper and lower rate constant limits of this elementary reaction alone yield differences in the mass burning rate of a factor of three at 30 atm. Likewise, the difference in predictions between the model of Li et al. and Davis et al. for the conditions of Fig. 4 can be attributed mainly to differences in rate constants used for (R1), (R5), and (R7). Fig. 19 reveals that substitution of the rate constants for those three reactions from Davis et al. into Li et al. results in nearly the same predictions as Davis et al. Therefore, even these three reaction rate constants or ratios of them are relatively unconstrained among validated models.

Furthermore, predictions at the conditions of this paper are sensitive to the third body collision efficiencies for bath gases and treatment of pressure dependence for (R1) since the reaction is

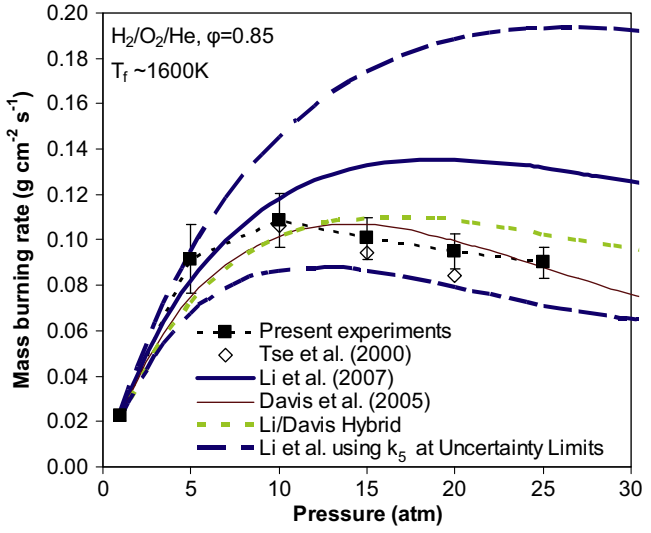

Fig. 19. Comparison of experimental data from present study and Ref. [10] and predictions using various models: the original model of Li et al. [17], the original model of Davis et al. [18], a hybrid model of Li et al. where the rate constants for (R1), (R5), and (R7) are substituted from Davis et al., and modified models of Li et al. that use rate constants for (R5) at the upper and lower uncertainty limits at 3500 K, ln (*A*) = 0.2, given by Baulch et al. [51]. The results demonstrate the increased sensitivity to the choice of rate constants for (R1), (R5), and (R7) in flames at higher pressures.

in the fall-off regime. Since a large amount of H_2O is formed throughout the flame and H_2O is an especially efficient collider, the flame predictions are strongly sensitive to the H_2O third body efficiency used in the model. The various kinetic models studied here [12,17–21,24] employ a range of values for the third body efficiency of H_2O relative to Ar from 16 to 24. Recent measurements of (R1) at 298 K [49] and 1050 to 1250 K [52] indicate an efficiency in the range of 20 to 23 relative to Ar. When a third body efficiency for H_2O of 24 is substituted in the model of Li et al., which uses 16, the predicted burning rate is lowered by 30% at 30 atm. Efficiency factors of other important bath gases such as CO_2 likely require further attention as well.

There are two main sources of uncertainty regarding the pressure dependence of (R1) under the present conditions. First, there is some variation among values proposed for the center broadening factors, F_c, in pure bath gases [51–56] – from 0.5 to 0.7 for Ar, 0.5 to 0.7 for N_2, and 0.6 to 0.8 for H_2O – and limited studies on other bath gases. Second, there is a lack of fundamental understanding of the mixing rules for fall-off reactions with bath gases having different broadening factors [16], which is especially important in flame studies and practical systems where there are appreciable concentrations of multiple species. To demonstrate the significance of the treatment of fall-off for (R1) for the present conditions, simulations were performed using the original model of Li et al. [17], which uses $F_c = 0.5$ for all colliders when the diluent is Ar or He, and a modified version of Li et al., which uses $F_c = 0.8$ (the recommended value for H_2O [51], which as a collider is responsible for a large portion of the flux through (R1)) for all colliders. For the lean H_2/O_2/He mixture of Fig. 4, the two models yield burning rates at 30 atm that are different by ~20%.

As discussed in the previous section, reaction rate constants of HO_2 with other radical species are strongly sensitive in a higher temperature window at higher pressures. There are relatively few elementary rate studies on the competing $HO_2 + H$ channels at temperatures of interest to combustion modeling. There is atmospheric temperature work (e.g. Refs. [57,58]) and experimental measurements of a ratio of the rate constants of reactions (R8), (R5) and $HO_2 + HO_2 = H_2O_2 + O_2$ (R17), and a ratio of the rate constants of reactions (R9), (R5) and (R17) at 773 K [59]. There is a recent theoretical expression and measurements in the 1600–2000 K temperature range for (R8), that suggest a stronger temperature dependence than used in many of the current models [60]. However, it appears that these reactions continue to have large uncertainties in their rate constants and temperature dependences and deserve further attention, particularly at temperatures above 1000 K.

Reaction (R10) has been primarily studied at atmospheric conditions (e.g. Refs. [61–64]) due to the significance of this reaction in the HO_x cycle of atmospheric chemistry. More recently, high temperature measurements [65,66] have shown that (R10) exhibits an uncommon and highly non-Arrhenius behavior, indicative of the formation of an activated complex. Experimental measurements of the rate constant of (R10) reveal a deep, narrow "well" around 1000 K (Ref. [66]) or 1200 K (Ref. [65]). Fig. 18 indicates that the temperature window of peak sensitivity to (R10) at pressures above 10 atm is located inside the temperature window where the local rate minimum of (R10) was observed. Therefore, accurate characterization of the rate constant of (R10) in this region is critical to predicting the burning rate of H_2/O_2 flames above ~10 atm.

In addition, the present level of understanding of elementary processes allow for the possibility that one or more elementary reactions that could be important in high-pressure H_2 flames but are not included in most of the current H_2 combustion models. For example, the reaction $O + OH + M = HO_2 + M$ (R15) is not included in almost all recent H_2 models [12,17–20] with the exception of that of Saxena and Williams [21,67] where the reaction was included only "for completeness." While the reaction was included in early mechanisms for H_2 ignition (e.g. [1,68]), (R15) has largely been concluded to be unimportant [1]. Elementary studies of (R15) are sparse and span orders of magnitude. A review by Bahn [69] cites studies that present values of $k_{15} = 1.2 \times 10^{17}$ cm^6/mol^2/s [70] and 5×10^{16} cm^6/mol^2/s [71]. In a more recent theoretical study, Germann and Miller [72] employed a flux–flux correlation function approach to calculate the rate constants for the competing O + OH reaction (H + O_2) and recombination (HO_2) channels. They arrive at a nearly temperature-independent rate constant of approximately $k_{15} = 10^{15}$ cm^6/mol^2/s. The values for k_{15} used in modeling studies (where the reaction has been included) have ranged from 8×10^{15} cm^6/mol^2/s [21] to 10^{17} cm^6/mol^2/s [1,68]. Inclusion of this reaction with the largest rate constant proposed in the literature, 10^{17} cm^6/mol^2/s [1,68], into the model of Li et al. [17] was tested against the validation targets of Ref. [16] – it does not substantially affect flow reactor species profiles up to 3.4 atm, ignition delays up to 87 atm, and rich flame speeds up to 20 atm, but it does affect lean flames especially at high pressures.

Fig. 20 compares burning rate predictions using the model of Li et al. modified to include (R15) for the range of values proposed for k_{15} (from 10^{15} to 10^{17} cm^6/mol^2/s) using the same collision efficiencies as those used for (R1). Inclusion of the reaction has minimal effect for lower values of k_{15}. If k_{15} is ~10^{16} or larger, the reaction reduces the predicted mass burning rate at higher pressures. At the upper limit of proposed rate constants (~10^{17} cm^6/mol^2/s), the reaction reduces the burning rate by up to 35%. Further studies on (R15) to reduce the uncertainty in the rate constant would be required to ascertain its effect on lean high pressure flames. At present however, it appears that $O + OH + M = HO_2 + M$ may in part be important to achieving more accurate burning rate predictions under the conditions of interest in this paper.

The large sensitivity to the competing channels of $H + HO_2$ might suggest that stabilization to H_2O_2 could be important under the present conditions. Stabilization of the excited adduct, $HOOH^*$, through which reaction (R9) proceeds, is part of the proposed mechanism for the $H + HO_2$ reaction discussed in Ref. [73], but the results of their theoretical treatment imply that the stabilization channel is insignificant.

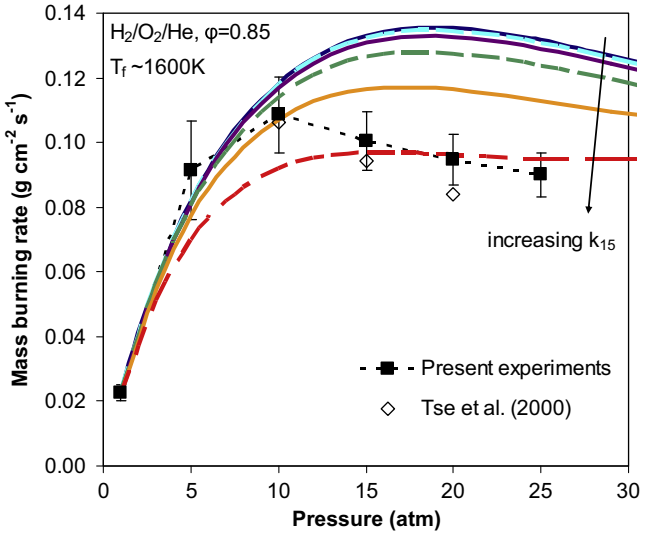

Fig. 20. Comparison of experimental data with predictions using the model of Li et al. [17] and a modified version of Li et al. that includes various rate expressions for $O + OH + M = HO_2 + M$ (R15) within the uncertainty limits for the reaction. The lines in order of decreasing burning rate magnitude are predictions using $k_{15} = 0$, 10^{15}, 3×10^{15}, 10^{16}, 3×10^{16}, and 10^{17} cm^6/mol^2/s.

Given the large sensitivity to rate constants of reactions that consume H atoms, one might also suspect that modeling difficulties could be attributed to H atom diffusion coefficients. In order to discern this effect, simulations of the lean conditions used in Fig. 4 were conducted using the model of Li et al. [17], where the Lennard-Jones collision diameter for H atom was artificially modified in the transport file. The modified collision diameter required to observe a difference in the predicted burning rate of even 5% was 3.2 times lower – resulting in a diffusion coefficient approximately 10 times higher. Such a small sensitivity of the predicted burning rate to diffusion coefficients is consistent with the observations of Zhao et al. [50]. They further noted that sensitivity to the diffusion coefficient is non-monotonic throughout the flame, such that the effect of a temperature-independent change in the diffusion coefficient largely cancels when integrated across the whole flame. However, a first-principle calculation by Middha et al. [74] suggest a stronger temperature dependence of the H atom diffusion coefficient than that obtained using the conventional TRANFIT [75] code – about 20% higher at 1500 K. Employing this treatment of H atom diffusion from [76] and the kinetic model of Li et al. in flame simulations yields predicted burning rates up to 10% higher at higher pressure compared to using TRANFIT. Thus, while the H atom diffusion coefficient contributes to the uncertainty in the predicted flame speed, it does not appear to be the main source of disagreement between predictions and experimental data.

At present, individual substitution of rate constants for the reactions discussed above from the recent literature ((R1) from Sellevåg et al. [55] and Pang et al. [77]; (R2) from Srinivasan and Michael [78] and Sellevåg et al. [55]; (R8) from Michael et al. [60]; (R10) from Chaos and Dryer [22]) as well as diffusion coefficients from [76] into Li et al. does not completely reconcile differences between model predictions and experimental data.

5. Conclusions

The pressure and flame temperature dependences of mass burning rates for $H_2/CO/O_2$/diluent mixtures have been studied experimentally and numerically. Flame speeds and mass burning rates were extracted from outwardly propagating flames for equivalence ratios from 0.85 to 2.5, pressures from 1 to 25 atm and flame temperatures of 1500 to 1800 K, CO fuel fractions from 0 to 0.9, and dilution concentrations of He up to 0.8, Ar up to 0.6, and CO_2 up to 0.4. The major conclusions are:

1. At low pressures, the mass burning rate is experimentally observed to increase with pressure, while at greater pressures, the mass burning rate is found to decrease with pressure for both lean and rich conditions. Negative pressure dependence of the mass burning rate is observed at lower pressures for mixtures with lower flame temperatures. Additionally, the temperature dependence of the burning rate increases substantially with pressure. Carbon monoxide addition to the fuel does not significantly alter the pressure dependence for CO fractions of 0.5 (compared to pure H_2 fuel at the same pressure and temperature). Dilution with CO_2 strengthens the pressure and temperature dependence.
2. While for low pressures or high flame temperatures, the various models employed in this study *all* yield predictions in good agreement with experimental data, *none* predicts the observed burning rate pressure dependence across all conditions. Large variations, up to a factor of three, are observed among the model predictions. Such large discrepancies among the model predictions are surprising given that all were validated against extensive (and frequently the same) data sets.
3. Simulations were performed to extend the experimentally studied conditions to conditions typical of gas turbine combustion in Integrated Gasification Combined Cycle processes. Preheating the mixture while increasing dilution to maintain the same flame temperature yields burning rate pressure dependence and sensitivity results nearly identical to the non-preheated case. Preheating the mixture with fixed dilution yields weakened burning rate pressure dependence and sensitivity results, in a manner similar to raising the flame temperature through decreasing dilution. Additionally, the strength of the burning rate pressure dependence of H_2/O_2/diluent flames can be ranked by diluent as $He < N_2 < CO_2 < H_2O$.
4. As the pressure is increased, the extended second limit, which demarcates straight-chain kinetics from chain-branching kinetics, is shifted to higher temperatures. Consequently, the portion of the flame zone in which strong branching occurs is restricted to a narrower, higher temperature window as pressure is increased – resulting in a shift of the peak for all radical species and reaction fluxes to higher temperatures. Indeed, sensitivity analysis shows that competing channels of the $H + O_2$ and $H + HO_2$ reactions, which largely govern the fate of H, are responsible for the pressure dependence for rich conditions. The same reactions are important for lean conditions in addition to $OH + H_2$ and $OH + HO_2$, which largely govern the fate of the OH radical.
5. The sensitivities of mass burning rates to elementary rate constants increase considerably with pressure. The large sensitivities at high pressures amplify the effects of uncertainties in rate constants for elementary reactions. As a result, the disagreement in burning rate predictions by various models can be attributed to uncertainties associated with a number of reactions, including HO_2 + radical reactions like (R8)–(R10), radical-radical recombination reactions like (R2) and (R15)–(R16), and even well-studied reactions like (R1) and (R5)–(R7). (See Table 2 for the list of reactions discussed.) The predictions at high pressures are additionally sensitive to collision efficiencies as well as the treatment of fall off for (R1).
6. The temperature window of peak sensitivity to rate constants moves to a narrower, higher temperature range with increasing pressure, most noticeably for reactions of HO_2 with H and OH. Given that these reactions have relatively large uncertainties in their rate constants and complex temperature dependencies, especially around and above 1000 K, it appears likely that these reactions are largely (though not completely) responsible for the disagreement among the models and with experimental data. Additional experimental and theoretical analyses on reactions (R8), (R9), and (R10) are needed to support resolution of model predictions at conditions important to syngas combustion at high pressures.
7. There appear to be one or more elementary reactions that could be important in high-pressure H_2 flames but are missing from most of the current H_2 combustion models. For example, the reaction $O + OH + M = HO_2 + M$ (R15) is not included in almost all H_2 models, but is demonstrated here to significantly impact predictions of lean high pressure flames using rate constants within their uncertainty limits.
8. Since recombination reactions are favored with increasing pressure and decreasing flame temperature, flux through recombination and branching channels can become roughly equal through the most reactive portion of the flame at high pressures and low flame temperatures. As a result, the sensitivity of the predictions to the rate parameters for those reactions increases dramatically. The elevated sensitivities to input parameters have two major implications. First, high pressure flames will be very difficult to model accurately – a given uncertainty in a rate parameter will result in a larger uncertainty in the flame

speed/burning rate at higher pressures. Second, validation against high pressure flame targets could be highly beneficial in the development of a model since the high pressure flame targets provide a stronger constraint on the model parameters.

9. Though this paper points to significant shortcomings in existing models and parameters could be varied to match predictions to experiments, more fundamental elementary reaction studies to better define the pressure and temperature dependences of the noted reactions are needed to elucidate a scientifically based solution. We are continuing efforts to achieve this result.

Acknowledgements

This work was supported by the US Department of Energy under DE-FG26-06NT 42716 (FLD, YJ) from the Pittsburgh National Energy Technology Laboratories and by Grant No. DE-FG02-86ER13503 (FLD) from the Chemical Sciences, Geosciences and Biosciences Division, Office of Basic Energy Sciences, Office of Science. Support from Siemens Power Generation, Inc., (technical monitor, Dr. Scott Martin) (FLD) and by the Petroleum Research Fund from American Chemistry Society under Grant PRF# 43460-AC5 (YJ) is also acknowledged. We wish to thank Dr. Timothy Ombrello for his assistance in improving the ignition assembly, other researchers in the Dryer and Ju groups for helpful discussions, and Prof. Hai Wang for supplying the updated transport database and interpreter.

Appendix A. Supplementary material

Supplementary data associated with this article can be found, in the online version, at doi:10.1016/j.combustflame.2009.08.009.

References

[1] C.K. Westbrook, F.L. Dryer, Prog. Energy Combust. Sci. 10 (1984) 1–57.
[2] G.A. Richards, K.H. Casleton, N.T. Weiland, Syngas utilization, in: T.C. Lieuwen, V. Yang, R.A. Yetter (Eds.), Synthesis Gas Combustion: Fundamentals and Applications, Taylor & Francis, 2009, pp. 193–222.
[3] M. Chaos, M.P. Burke, Y. Ju, F.L. Dryer, Syngas chemical kinetics and reaction mechanisms, in: T.C. Lieuwen, V. Yang, R.A. Yetter (Eds.), Synthesis Gas Combustion: Fundamentals and Applications, Taylor & Francis, 2009, pp. 29–70.
[4] D.R. Dowdy, D.B. Smith, S.C. Taylor, A. Williams, Proc. Combust. Inst. 23 (1990) 325–332.
[5] K.T. Aung, M.I. Hassan, G.M. Faeth, Combust. Flame 109 (1997) 1–24.
[6] L. Qiao, Y. Gu, W.J.A. Dahm, E.S. Oran, G.M. Faeth, Combust. Flame 151 (2007) 196–208.
[7] I.C. McLean, D.B. Smith, S.C. Taylor, Proc. Combust. Inst. 25 (1994) 749–757.
[8] M.I. Hassan, K.T. Aung, G.M. Faeth, J. Propul. Power 13 (1997) 239–245.
[9] C.M. Vagelopoulos, F.N. Egolfopoulos, Proc. Combust. Inst. 25 (1994) 1317–1323.
[10] S.D. Tse, D.L. Zhu, C.K. Law, Proc. Combust. Inst. 28 (2000) 1793–1800.
[11] D. Bradley, M. Lawes, K. Liu, S. Verhelst, R. Woolley, Combust. Flame 149 (2007) 162–172.
[12] H.Y. Sun, S.I. Yang, G. Jomaas, C.K. Law, Proc. Combust. Inst. 31 (2007) 439–446.
[13] J. Natarajan, T. Lieuwen, J. Seitzman, Combust. Flame 151 (2007) 104–119.
[14] J. Natarajan, Y. Kochar, T. Lieuwen, J. Seitzman, Proc. Combust. Inst. 32 (2009) 1261–1268.
[15] M.A. Mueller, T.J. Kim, R.A. Yetter, F.L. Dryer, Int. J. Chem. Kinet. 31 (1999) 113–125.
[16] J. Li, Z. Zhao, A. Kazakov, F.L. Dryer, Int. J. Chem. Kinet. 36 (2004) 566–575.
[17] J. Li, A. Kazakov, Z. Zhao, M. Chaos, F.L. Dryer, J.J. Scire, Int. J. Chem. Kinet. 39 (2007) 109–136.
[18] S.G. Davis, A. Joshi, H. Wang, F.N. Egolfopoulos, Proc. Combust. Inst. 30 (2005) 1283–1292.
[19] A.A. Konnov, Combust. Flame 152 (2008) 507–528.
[20] M. O'Connaire, H.J. Curran, J.M. Simmie, W.J. Pitz, C.K. Westbrook, Int. J. Chem. Kinet. 36 (2004) 603–622.
[21] P. Saxena, F.A. Williams, Combust. Flame 145 (2006) 316–323.
[22] M. Chaos, F.L. Dryer, Combust. Sci. Technol. 180 (2008) 1051–1094.
[23] J. Natarajan, T. Lieuwen, J. Seitzman, J. Eng. Gas Turb. Power 130 (2008) 061502-1.
[24] G.P. Smith, D.M. Golden, M. Frenklach, N.W. Moriarty, B. Eiteneer, M. Goldenberg, C.T. Bowman, R.K. Hanson, S. Song, W.C. Gardiner Jr., V.V. Lissianski, Z. Qin, GRI-MECH 3.0. <http://www.me.berkeley.edu/gri_mech/>.
[25] Z. Chen, M.P. Burke, Y. Ju, Proc. Combust. Inst. 32 (2009) 1253–1260.
[26] M.P. Burke, Z. Chen, Y. Ju, F.L. Dryer, Combust. Flame 156 (2009) 771–779.
[27] Z. Chen, M.P. Burke, Y. Ju, Combust. Theory Model. 13 (2009) 343–364.
[28] X. Qin, Y. Ju, Proc. Combust. Inst. 30 (2005) 233–240.
[29] R.K. Tepe, D. Vassallo, T. Jacksier, R.M. Barnes, Spectrochim. Acta B 54 (1999) 1861–1868.
[30] D. Reinelt, G.T. Linteris, Proc. Combust. Inst. 26 (1996) 1421–1428.
[31] G.T. Linteris, M.D. Rumminger, V.I. Babushok, Prog. Energy Combust. Sci. 34 (2008) 288–329.
[32] T.C. Williams, C.R. Shaddix, Combust. Sci. Technol. 175 (2008) 1225–1230.
[33] R.A. Strehlow, L.D. Savage, Combust. Flame 31 (1978) 209–211.
[34] J.R. Kee, F.M. Rupley, J.A. Miller, Sandia National Laboratories Report SAND 89-8009B, Livermore, CA, 1992.
[35] G.H. Markstein, Non-Steady Flame Propagation, Pergamon, New York, 1964. p. 22.
[36] A.P. Kelley, C.K. Law, Combust. Flame 156 (2009) 1844–1851.
[37] G. Rozenchan, D.L. Zhu, C.K. Law, S.D. Tse, Proc. Combust. Inst. 29 (2002) 1461–1469.
[38] G. Jomaas, J.K. Bechtold, C.K. Law, Proc. Combust. Inst. 31 (2007) 1039–1046.
[39] L. Qiao, Y. Gu, W.J.A. Dahm, E.S. Oran, G.M. Faeth, Proc. Combust. Inst. 31 (2007) 2701–2709.
[40] F.N. Egofopoulos, C.K. Law, Combust. Flame 80 (1990) 7–16.
[41] F.N Egofopoulos, Ph.D. Thesis, Princeton University, 1990.
[42] C.K. Law, Combustion Physics, Cambridge University Press, New York, 2006.
[43] Z. Chen, M.P. Burke, Y. Ju, in: Society for Industrial and Applied Mathematics: 12th International Conference on Numerical Combustion, 2008.
[44] Z. Chen, X. Qin, B. Xu, Y. Ju, F. Liu, Proc. Combust. Inst. 31 (2007) 2693–2700.
[45] H. Guo, Y. Ju, K. Maruta, T. Niioka, F. Liu, Combust. Sci. Technol. 135 (1998) 49–64.
[46] B. Lewis, G. von Elbe, Combustion, Flames and Explosions of Gases, third ed., Academic Press, Orlando, 1987.
[47] M.A. Mueller, T.J. Kim, R.A. Yetter, F.L. Dryer, Fall Meeting of the Eastern States Section of the Combustion Institute, Hilton Head Island, SC, December 1996.
[48] X.L. Zheng, C.K. Law, Combust. Flame 136 (2004) 168–179.
[49] J.V. Michael, M.-C. Su, J.W. Sutherland, J.J. Carrroll, A.F. Wagner, J. Phys. Chem. A 106 (2002) 5297–5313.
[50] Z. Zhao, J. Li, A. Kazakov, F.L. Dryer, Int. J. Chem. Kinet. 37 (2005) 282–295.
[51] D.L. Baulch, C.T. Bowman, C.J. Cobos, R.A. Cox, T. Just, J.A. Kerr, M.J. Pilling, D. Stocker, J. Troe, W. Tsang, R.W. Walker, J. Warnatz, J. Phys. Chem. Ref. Data 34 (3) (2005) 757–1397.
[52] R.W. Bates, D.M. Golden, R.K. Hanson, C.T. Bowman, Phys. Chem. Chem. Phys. 3 (2001) 2337–2342.
[53] C.J. Cobos, H. Hippler, J. Troe, J. Phys. Chem. 89 (1985) 342–349.
[54] J. Troe, Proc. Combust. Inst. 28 (2000) 1463–1469.
[55] S.R. Sellevåg, Y. Georgievskii, J.A. Miller, J. Phys. Chem. A 112 (2008) 5085–5095.
[56] R.X. Fernandes, K. Luther, J. Troe, V.G. Ushakov, Phys. Chem. Chem. Phys. 10 (2008) 4313–4321.
[57] U.C. Sridharan, L.X. Qiu, F. Kaufman, J. Phys. Chem. 86 (1982) 4569–4574.
[58] L.F. Keyser, J. Phys. Chem. 90 (1986) 2994–3003.
[59] R.R. Baldwin, R.W. Walker, J. Chem. Soc. Faraday Trans. I 75 (1979) 140–154.
[60] J.V. Michael, J.W. Sutherland, L.B. Harding, A.F. Wagner, Proc. Combust. Inst. 28 (2000) 1471–1478.
[61] W.B. DeMore, J. Phys. Chem. 83 (1979) 1113–1118.
[62] W.B. DeMore, J. Phys. Chem. 86 (1982) 121–126.
[63] U.C. Sridharan, L.X. Qiu, F. Kaufman, J. Phys. Chem. 88 (1984) 1281–1282.
[64] L.F. Keyser, J. Phys. Chem. 92 (1988) 1193–1200.
[65] H. Hippler, H. Neubauer, J. Troe, J. Phys. Chem. 103 (1995) 3510–3516.
[66] C.H. Kappel, K. Luther, J. Troe, Phys. Chem. Chem. Phys. 4 (2002) 4392–4398.
[67] <http://maeweb.ucsd.edu/~combustion/cermech/sandiego20051201.txt>.
[68] E.S. Oran, T.R. Young, J.P. Boris, A. Cohen, Combust. Flame 28 (1982) 135–148.
[69] G.S. Bahn, Reaction Rate Compilation for the H–O–N System, Gordon and Breach, New York, 1968. p. 113.
[70] C.B. Kretschmer, Investigation of Atomic Oxygen Recombination Rates, Aerojet-General Corporation Report 1611 (AFOSR-TR-59-62), AD 217008, May 1959.
[71] H.L. Petersen, C.B. Kretschmer, Kinetics of Recombination of Atomic Oxygen at Room Temperature, Aerojet-General Corporation Report TN-38 (AFOSR-TN-60-1478), AD 283044, November 1960.
[72] T.C. Germann, W.H. Miller, J. Phys. Chem. A 101 (1997) 6358–6367.
[73] S.H. Mousavipou, V. Saheb, Bull. Chem. Soc. Jpn. 80 (2007) 1901–1913.
[74] P. Middha, B. Yang, H. Wang, Proc. Combust. Inst. 29 (2002) 1361–1369.
[75] R.J. Kee, G. Dixon-Lewis, J. Warnatz, M.W. Coltrin, J.A. Miller, Sandia National Laboratories Report SAND 86-8246, Livermore, CA, 1986.
[76] H. Wang, X. You, A.V. Joshi, S.G. Davis, A. Laskin, F. Egolfopoulos, C.K. Law, USC Mech Version II. High-Temperature Combustion Reaction Model of H2/CO/C1-C4 Compounds, May 2007. <http://ignis.usc.edu/USC_Mech_II.html>.
[77] G.A. Pang, D.F. Davidson, R.K. Hansen, Proc. Combust. Inst. 32 (2009) 181–188.
[78] N.K. Srinivasan, J.V. Michael, Int. J. Chem. Kinet. 38 (2006) 211–219.